



Current treatment of bulk single wall carbon nanotubes to heal defects without structural change for increased electrical and thermal conductivities

Journal:	<i>Nanoscale</i>
Manuscript ID:	NR-COM-01-2015-000170.R1
Article Type:	Communication
Date Submitted by the Author:	12-Feb-2015
Complete List of Authors:	Matsumoto, Naoyuki; AIST, Oshima, Azusa; AIST, Yumura, Motoo; AIST, Futaba, Don N.; AIST, Hata, Kenji; AIST,

Current treatment of bulk single wall carbon nanotubes to heal defects without structural change for increased electrical and thermal conductivities

Naoyuki Matsumoto^a, Azusa Oshima^a, Motoo Yumura^{a, b}, Don N. Futaba^{,a, b}
and Kenji Hata^{*,a, b}*

Affiliation

^a Technology Research Association for Single Wall Carbon Nanotubes (TASC), Central 5, 1-1-1 Higashi, Tsukuba, Ibaraki 305-8565, Japan

^b National Institute of Advanced Industrial Science and Technology (AIST), Central 5, 1-1-1 Higashi, Tsukuba, Ibaraki 305-8565, Japan

*Corresponding authors. Tel/Fax: +81 29-861-4851. E-mail: d-futaba@aist.go.jp (D. N. Futaba), kenji-hata@aist.go.jp (K. Hata).

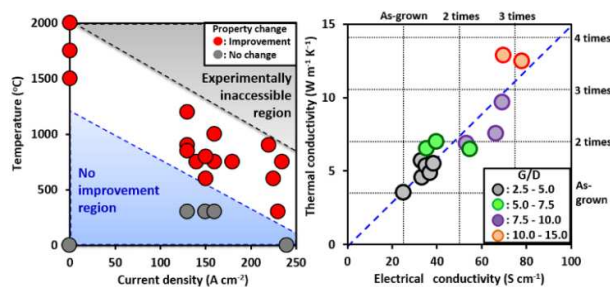
ABSTRACT

By applying electrical current with heat, we succeeded in improving the graphitization of single wall carbon nanotubes (SWCNTs) without increasing the diameter and wall number. At 800 °C, 150 A cm⁻² (1150 W cm⁻²) for 1 min, we achieved a 3.2-times increase in Raman G- to D-band ratio, a 3.1-times increase in electrical conductivity (from 25.2 to 78.1 S cm⁻¹), a 3.7-times increase in thermal conductivity (from 3.5 to 12.8 W m⁻¹ K⁻¹), and even a 1.7-times increase in dispersibility (from 1.7 to 2.9 mg L⁻¹). The electrical and thermal conductivities did not only increase simultaneously, but relative increases for the electrical and thermal conductivities were identical across our experimental range, that stems from defect healing without change in diameter and wall number. In contrast, a significant increase in diameter and wall number was observed when current was not applied. These results demonstrate the importance of applying current to improve the graphitization of SWCNTs while maintaining their structure as SWCNTs.

Keywords

Single walled carbon nanotube, Post-synthetic process, Current treatment, Heat treatment, Thermal conductivity, Electrical conductivity

TOC GRAPHICS



No practical material can be free from defects, and in many cases defects represent the bottleneck for the application of a material. For example, the development of carbon fibers was a 40 year struggle against defects to improve the fabrication process to first remove the micron-scale, then the sub-micron-scale, and finally the nanoscopic defects.¹⁻³ At each level, when the defects were removed, the tensile strength of carbon fibers increased from ~2 GPa and finally reaching ~10 GPa, and now has reached the current status where the aircrafts are largely composed of carbon fiber composites.²⁻⁴ However, even with the most advanced modern technologies, carbon fibers contain a high level of atomistic defects as evidenced by the fact that the structure cannot be defined at the atomic scale.

In contrast, single wall carbon nanotubes (SWCNTs) have the potential to possess a perfect structure down to the atomic-scale, because the chemical structure can be completely defined by its chirality. However, in practice, SWCNTs include many defects. For example, an ideal SWCNT is predicted to possess a tensile strength of ~400 GPa but experimental on macroscopic fibers have only demonstrated tensile strengths of ~3 GPa.⁵⁻⁷ Similarly, the thermal conductivity for SWCNTs is expected to be ~6600 W m⁻¹ K⁻¹ at room temperature, but the thermal conductivity of a SWCNT bundle (diameter: 10nm) has only been measured to be ~150 W m⁻¹ K⁻¹ at room temperature.⁸⁻⁹ In addition, the ampacity has been theoretically estimated to be as high as 10¹³ A cm⁻² but only 10⁷–10⁹ A cm⁻² has been measured.¹⁰⁻¹² SWCNTs grown by high temperature processes, like arc discharge and laser ablation, have been shown to be relatively defect-free, but SWCNTs grown by chemical vapor deposition (CVD) have shown to contain more defects, and this fact is acknowledged as a significant bottleneck for their usage.¹³⁻¹⁵ CVD technology has improved over the decades, and a few approaches have succeeded in growing SWCNTs with high crystallinity.¹⁶⁻¹⁸ However, in general, high crystallinity results in a reduction in yield as demonstrated by the inverse relationship between the crystallinity and the yield.¹⁹

Therefore, significant effort has been invested to develop post processes of CNTs to remove the defects created during the synthesis stage analogous to the treatment of carbon fibers. Post processes as represented by high temperature treatments, the standard post process for carbon fibers, have been successfully adopted for multi-walled carbon nanotubes (MWCNTs).² For example, Showa Denko K.K. has improved the crystallinity of their MWCNTs-vertically grown carbon fibers (VGCFs) (diameter: 150 nm) by the Addison high temperature treatment and succeeded in commercializing them for use in Li-ion batteries, representing one of the most significant applications of CNTs.²⁰

From a scientific standpoint, there have been a number of reports on the heat treatment of CNTs. For example, Mattia *et al.* reported the heat treatment of MWCNTs at 1200–2000 °C and reported an increase in Raman G- to D-band ratio (an indicator of crystallinity) and a two-times improvement in the electrical properties.²¹ Zhao and Jin *et al.* demonstrated the rapid graphitizing of MWCNTs at 2000–2800 °C in an argon (Ar) atmosphere resulting in an improvement in CNT purity and the crystallinity, and a ~2.0 and ~1.5 times increase in the electrical conductivity and thermal diffusivity, respectively.^{22, 23} In addition, Musso *et al.* annealed a vertically aligned MWCNT mat at 1500–2000 °C in an Ar ambient achieving an increase in stiffness and macroscopic compressive strength.²⁴

When SWCNTs are exposed to similar high temperature processes (“heat only” processes), improvement in the crystallinity has been reported, but simultaneously it invokes a structural change in terms of an increase in both diameter and wall number.²⁵⁻²⁸ This is a critical problem because a wall number increase for SWCNTs means that they are no longer SWCNTs. For example, Yudasaka *et al.* reported the heating of SWCNTs (HiPCO) at 1000–2400 °C in a vacuum and Ar, and the diameter and wall number of the SWCNTs increased to double-walled CNTs (DWCNTs) and even MWCNTs at temperatures above 1900 °C.^{25, 26} Molecular dynamics simulations by Lopez *et al.* have shown that the diameter and wall

number increases due to the thermal coalescence of adjacent SWCNTs by a physical “patching-and-tearing” mechanism.^{27,28} Therefore, to date, there has been no post growth processes that can remove the defects and improve the SWCNT crystallinity without also increasing the diameter or wall number.

In this article, to address this important issue, we propose an original post-process where electrical current (current density: $\sim 240 \text{ A cm}^{-2}$, Electrical power density: $\sim 2000 \text{ W cm}^{-2}$) was passed current through a macroscopic SWCNT sheet at high temperatures (room temperature to $\sim 2000 \text{ }^\circ\text{C}$) (Fig. 1a). This process was enabled by controlling thermal expansion and electrical discharge associated with these severe conditions. Importantly, we found this treatment could selectively remove the defects while preserving the diameter and wall number, a result which differs from heat-only treatments which result in increases in both the diameter and wall number. As a result, we observed a 3.1-times improvement in the crystallinity (Raman G- to D band ratio from 4.2 to 13.1), a 3.1-times increase in electrical conductivity, a 3.7-times increase in thermal conductivity, and a 1.7-time increase in dispersibility. We believe that it is significant that an improvement was observed in every important aspect to use the treated SWCNTs for real applications, and thus could open up an opportunity to achieve highly graphitized and high performance SWCNTs from economical and high production synthesis processes.

Thermal expansion and electrical discharge were obstacles in applying high current densities at elevated high temperatures. For example, insufficient contact between the electrodes and sample easily resulted in electrical discharge; furthermore, if the electrodes and sample were first placed in contact and heated, thermal expansion of the electrodes would cause damage to both the samples and electrodes. Moreover, when high electrical current was passed through the CNTs, the local temperature further increases which invokes additional thermal expansion. These issues not only prevented the progression of experiments, but also made it impossible to achieve consistent and reproducible experimental results because the

contact resistance between the CNTs and electrodes varied due to variations in samples and treatment condition.

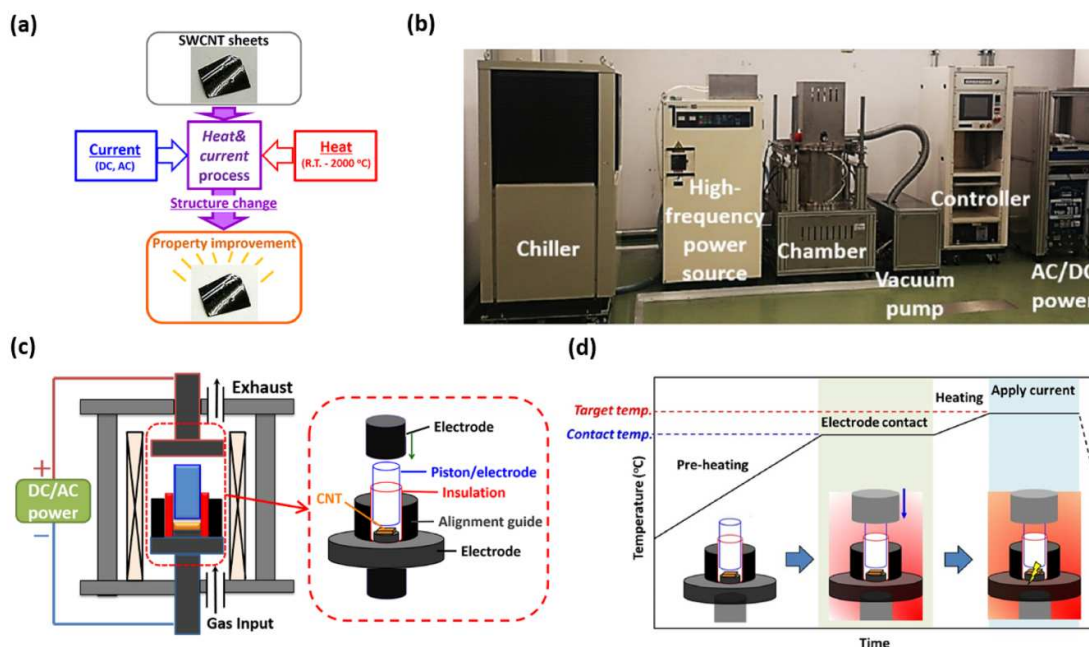


Fig. 1 (a) Conceptual representation of the *heat¤t* post-synthesis process. (b) Digital photograph of the device. (c) Schematic representation of the primary interior components. Inset: Sample treatment zone, and (d) treatment process.

In order to overcome these problems, we developed custom-made equipment that could pass through large electrical current densities through the SWCNTs at various ambient while maintaining high temperatures (Fig. 1b). The equipment was composed of vacuum chamber equipped with a high frequency induction heating system, isotropic carbon electrodes that treated samples of $10 \times 10 \text{ mm}^2$, and connected to a high current (both DC and AC) power supplies (Fig. 1c). Our equipment could perform treatments at different ambient (vacuum, neutral gases, and H_2) and apply currents up to 266 A at 120 V, at elevated temperatures up to 2000 °C. The key technology developed was the two probe electrodes with co-planar contact surfaces where the one was fixed while the other could be advanced by stepper-motor at desired positions for spacing adjustment. First, the electrodes were brought to a close distance

(~5.0 mm) without contact and the temperature was raised to ~30 °C below the target temperature to allow for thermal expansion. Second, while measuring the electrical resistance between the two electrodes (infinite at the beginning), the upper electrode was slowly moved towards the SWCNT and lower electrode and stopped when achieving a resistance of one ohm (Fig. 1d). In this way, we could achieve a very reliable and reproducible soft contact between the SWCNT sheets at different high temperatures.

SWCNTs (diameter: 2.9 nm, carbon purity: > 99.9 %, CNT purity: 93–95 %) were vertically aligned forests synthesized by the water-assisted chemical vapor deposition (Super-Growth CVD) method. SWCNTs were virtually free from metal impurities that would have seriously influenced the experimental results as previously reported.²⁹ The SWCNT forest was removed from the substrate, and the SWCNTs were laid flat into an aligned SWCNT sheet possessing a high density and two flat parallel surfaces, an important point to avoid poor electrical contact with the electrodes. It should also be noted that the orientation of the SWCNTs in the “aligned SWCNT sheet” were virtually perpendicular to the current flow.

We found that passing electrical current at high temperatures (“*heat¤t*” treatment) through the SWCNT sheets could improve the crystallinity by healing defects without causing increase to the diameter and wall number, while significantly improving electrical and thermal conductivities. The best treatment condition was found to be 150 A cm⁻² (1150 W cm⁻²) at 800 °C for 1 min in Ar gas flowing (1000 sccm) as determined by the increase in electrical and thermal conduction. Transmission electron microscope (TEM) images of the *heat¤t* SWCNTs compared to the as-grown SWCNTs showed an increase in straightness of the wall that indicated defect healing (Fig. 2a). In addition, the average diameter and wall number of the as-grown SWCNTs (diameter: ~2.9 nm, wall number: 1.0) and *heat¤t* SWCNTs were virtually unchanged. Macro-Raman spectroscopy (Fig. 2b) (sampling area: 100 μm) of the *heat¤t* SWCNTs compared to the as-grown SWCNTs showed an increased graphitic-to-disorder band (Raman G- to D-band) ratio from ~4.2 (as-grown) to ~13.1 (*heat¤t*) and a

higher G- to D-band ratio than that for only *heat*-treated SWCNTs (Fig. 2b). The increase in the Raman G- to D-band ratio indicates an improvement in the SWCNT graphitization, which is in agreement with the TEM results showing straighter SWCNTs. Further, comparison of the radial breathing mode spectra (RBM) for the as-grown, *heat*, and *heat¤t* SWCNTs showed identical peaks and intensities providing evidence of no change to the diameter.

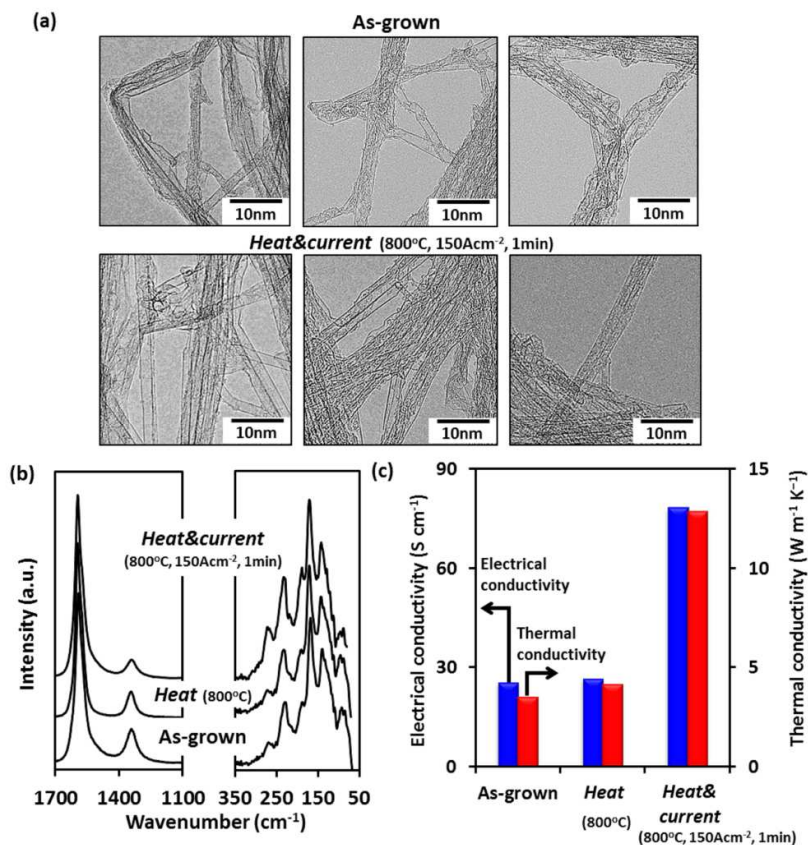


Fig. 2 (a) Transmission electron microscope images, (b) Raman spectra, and (c) electrical and thermal conductivities of the as-grown, *heat* and *heat¤t* treated SWCNTs.

Significantly, we observed an increase in both the electrical and thermal conductivities of the *heat¤t* treated SWCNTs compared with the as-grown and *heat*-only treated SWCNTs, *i.e.* comparing to as-grown SWCNTs, the thermal conductivity increased ~ 3.7 times from 3.5 to 12.8 W m⁻¹ K⁻¹ and the electrical conductivity increased ~ 3.1 times from 25.2 to 78.1 S cm⁻¹ (Fig. 2c). The electrical conductivity was measured by the four probe method, and the thermal conductivity was calculated from the thermal diffusivity, measured by thermowave

analysis, specific heat and density. We think that the simultaneous increase in both the thermal and electrical conductivity is important and results from defect healing without structural change. Electrical and thermal conductivity have a complex dependence on the diameter and wall number and typically do not increase simultaneously. For example, an increase in the diameter and wall number has shown increase in the electrical conductivity but not the thermal conductivity.^{30,31}

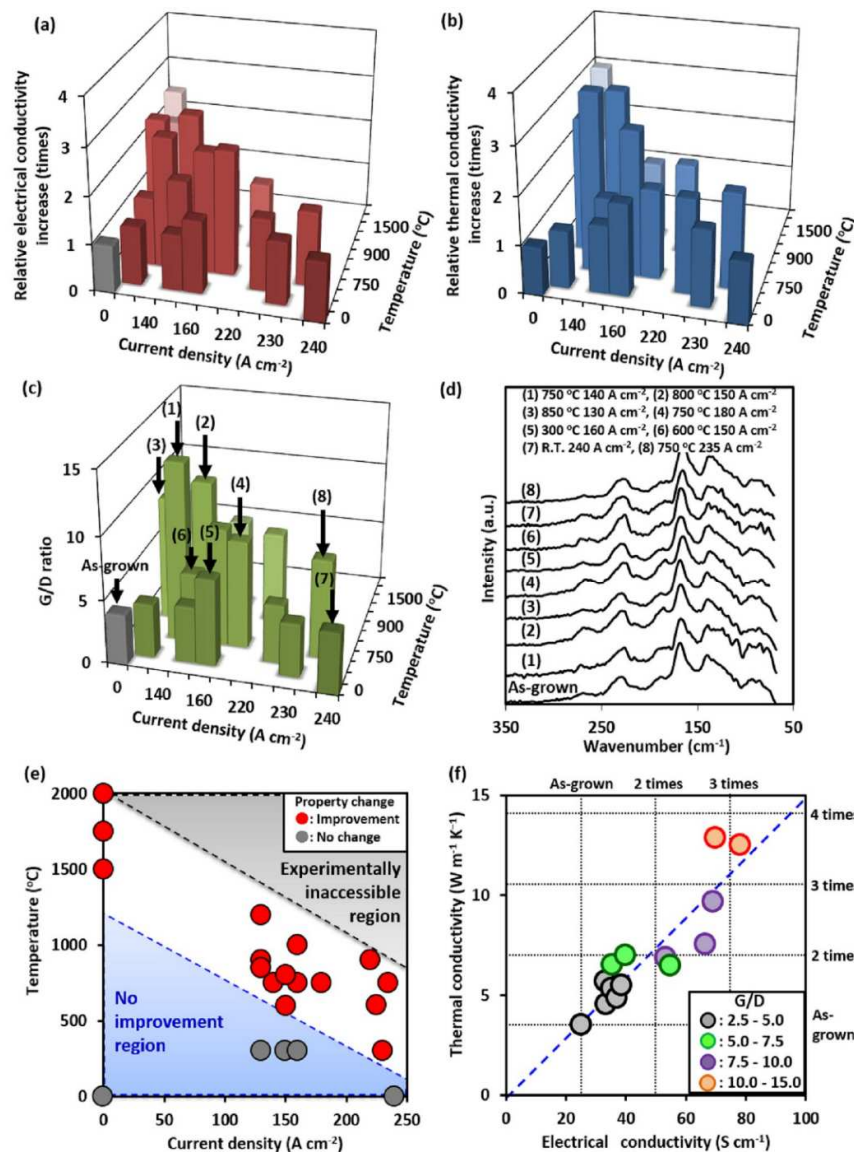


Fig. 3 3-D Mapping of the (a) electrical and (b) thermal conductivities and (c) G- to D-band ratios. (d) Radial breathing mode spectra. (e) 2-D mapping of the treatment region. (f) Ashby map of the electrical and thermal property improvement.

Since the thermal expansion and electrical discharge were controlled, the experimental results were reliable and reproducible. This enabled the mapping of the dependence of properties (electrical and thermal conductivities, Fig. 3a, 3b) and the structure (Raman G- to D-band ratio, Fig. 3c) as functions of the temperature (room temperature to 2000 °C) and electrical current density [0 to 240 A cm⁻² (2000 W cm⁻²)]. The Raman RBM spectra at each of these experimental treatment conditions showed identical profiles providing strong indication that the diameter of the SWCNTs was unaffected (Fig. 3d). The two-dimensional plots showed the experimental treatment range with the electrical current density on the x-axis, the temperature on the y-axis, the origin being the as-grown material (Fig. 3e). The high current density-high temperature region (grey) was inaccessible due to experimental limitations and the low-current density-low temperature region (blue) resulted in no change. There are several important results which arise from these mappings. First, we observe a range in the experimental treatment region centered at 800 °C and 150 A cm⁻² (1150 W cm⁻²) where a significant improvement was observed in all aspects, *i.e.* graphitization change, electrical conductivity and thermal conductivity. Second, when the current treatment was carried out without heating, even when applying the maximum current density, we only observed a minimal change in the structure which highlights the importance of the combination of both heating and electrical treatments. Third, the overall dependencies of each of the mappings followed a similar behavior, characterized by a single peak (positioned at the same experimental condition for each map), like the apex of a mountain, surrounded by a steady decrease in all directions.

We found that we could deepen our understanding by rearranging the maps into two Ashby plots where the x- and y-axes were the absolute value and relative values of the electrical and thermal conductivities, respectively, with colors indicating the Raman G- to D-band levels of Raman spectra (Fig. 3f). Interestingly, we found that the data fell on to a single straight line with slope one. This behavior would not occur if the electrical and thermal

conductivities changes were influenced by changes in diameter and wall numbers since the structural dependence on these properties differ.³¹ Therefore, we take this experimental results as direct evidence that the property change reflect an improvement in the crystallinity arising from defect healing induced by the heat treatment and electrical current flow.

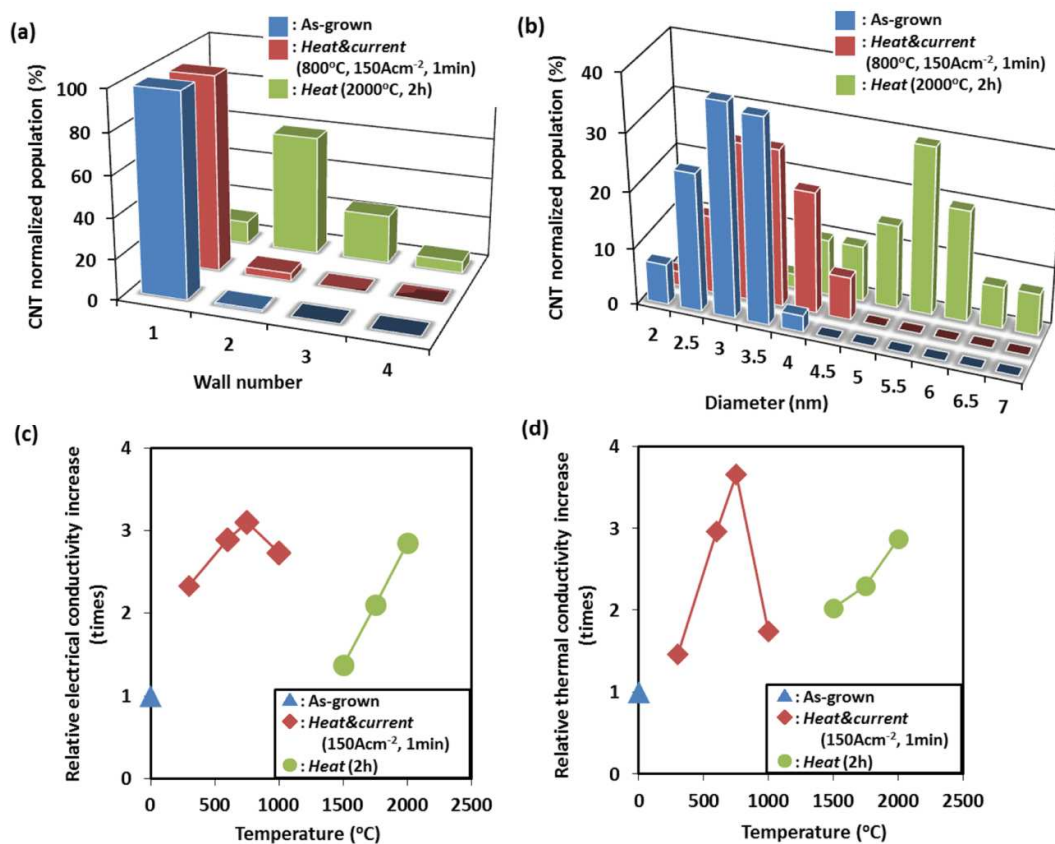


Fig. 4 Histograms of the (a) wall number and (b) diameter distribution. Process temperature effect on (c) electrical and (d) thermal conductivities.

To understand the contribution of current treatment, we compared the results of the *heat¤t* treatment to the *heat* only treatment. In contrast to the *heat¤t* treatment (at the optimum current density), the SWCNT sheet treated only by heat showed significant change. To demonstrate this, we plotted histograms of the wall number and diameter, as analyzed by TEM, for the as-grown, *heat¤t* (800 °C, 150 A cm⁻², 1 min, in Ar), and *heat* (2000 °C, 2 h in Ar) SWCNT sheets (Fig. 4a, 4b). The distribution of the diameter and

wall number for the *heat¤t* treated SWCNT sheets were nearly identical providing direct evidence that the *heat¤t* treatment did not invoke changes to the diameter and wall number. In contrast, the *heat* treated SWCNT sheets showed a significant increase in both average diameters, from ~2.9 nm to ~5.0 nm, and average wall number from ~1.0 to ~2.4. To be clear, SWCNT sheets treated by *heat* only were no longer SWCNTs. Further comparison of the *heat¤t* (at the optimum current density) and *heat* treatment was carried out by plotting the increases in electrical conductivity and thermal conductivity versus the heat treatment temperature (Fig. 4c, 4d). Both methods did increase both properties, but in both cases, the *heat¤t* treatment method achieved a higher improvement. Furthermore, the required *heat¤t* treatment process temperature was over ~900 °C lower than that for the *heat* only treatment.

While the precise mechanism of defect healing without structural change is unknown, we will provide a tentative explanation. It is well known that electrons ballistically transport through SWCNTs but are scattered significantly at defect sites.^{32, 33} This means that when electrons are passed through CNTs, the major resistance originates from the defect sites, and most of the consumption of the energy is concentrated at those locations. TEM observation has shown that electrons can induce structural changes at the defect sites, commonly known as the knock-on phenomenon.³⁴ More directly, *in-situ* TEM observations of SWCNTs with a current flow have shown defect healing invoked by the passage of electrical current.³⁵ Further, defects caused by the knock-on damage have been observed to migrate and coalesce.³⁶ We interpret that a similar process is occurring locally at the defect sites for the *heat¤t* treatment resulting in defect healing. In contrast, for *heat* treatments the energy is distributed uniformly to every atom and not locally to the defect sites. We interpret that this difference is the reason why we see no change in diameter and wall number for the *heat¤t* treatment, but do so for the *heat* treatment. Furthermore, previous reports have attributed the improvement of electrical conductivity of SWCNT buckypapers exposed to a thermal

treatment on the improvement of inter-tube contacts.^{21-23,26} However, in these reports, the thermal treatment was used for both carbonaceous impurity removal as well as defect healing, and so the removal of impurities results in a measurable decrease in mass and would likely result in improved inter-tube contacts. As discussed above, the purity of our samples is exceptionally high, and we do not observe a measurable change in mass after *heat¤t* treatment. Therefore, we attribute the improvement in properties to the improvement in crystallinity.

As the dispersion of SWCNTs represents an important process for the CNT material to be used in applications, the effect of *current&heat* treatment on the dispersion was characterized. In general, as the SWCNTs are laid down to form a solid sheet, a significant decrease in dispersibility was expected which would prevent applying the treated SWCNTs to real applications. To this end, a family of SWCNT dispersions was prepared by high pressure jet milling (60 MPa) of SWCNTs (as-grown, heat treated at 1500, 1750, 2000 °C for 2 h, and *heat¤t* SWCNT at 800 °C and 150 A cm⁻² for 1 min) in methyl isobutyl ketone (MIBK). Jet milling was chosen because it has shown to efficiently exfoliate the CNTs while minimizing damage.³⁷ Raman spectroscopy of the samples before and after dispersion showed no change in the G-band to D-band ratio and RBM spectra, directly showing that the jet milling dispersion did not induce observable damage to the SWCNTs (Supplemental Fig. S1). The ability to disperse was quantified as the concentration of SWCNTs in the dispersed solution from ultraviolet-visible (UV-vis) absorbance (Fig. 5). We found that the dispersibility significantly decreased (~50%) for the *heat* treated SWCNTs. In difference, and contrast to our expectation, we found that the dispersibility of the *heat¤t* treated SWCNT sheets did not decrease, but instead increased 1.7-times compared with the as-grown SWCNTs. At this moment, we do not completely understand the underlying reason for this phenomenon. Since the density of the *heat¤t* treated SWCNT sheets was ~10-times higher than that of the SWCNT forests, the Van der Waals interaction between the CNTs should be stronger

and resulting in decreased dispersibility. We hope that these results will invoke further studies to understand this important point.

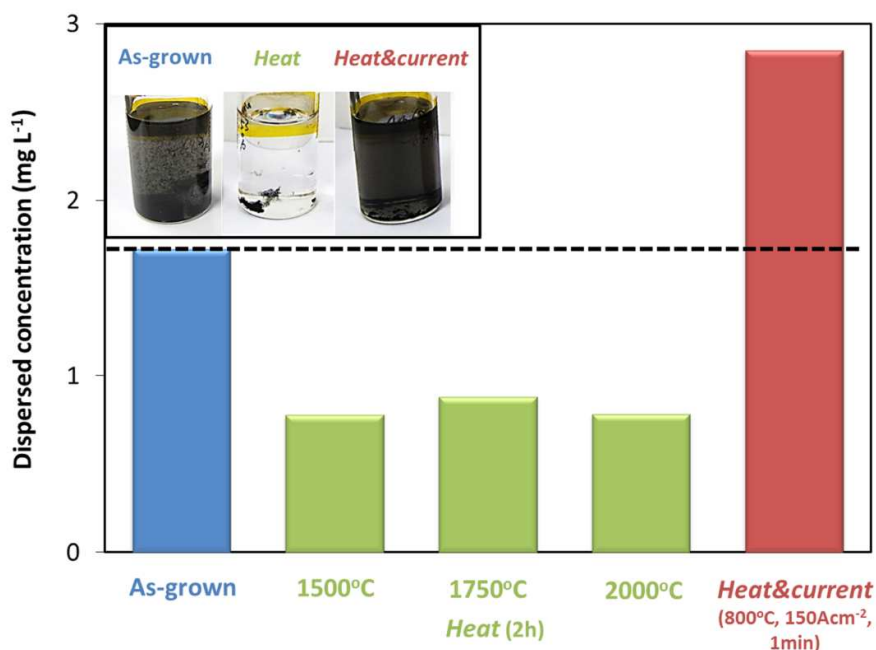


Fig. 5 Plot of the dispersed SWCNT concentration for different treatments. Inset: Digital photograph of dispersions.

Conclusions

We have developed a post-synthetic process for SWCNTs where electrical current was applied at high temperatures to selectively remove the defects without invoking change in the structure. The application of current was crucial to prevent an increase in diameter and wall number, therefore preserving SWCNTs as SWCNTs. Importantly, we found an improvement of performance in every important aspect for real applications. At the optimum process conditions, a 3.2-times increase in Raman G- to D-band ratio, a 3.1-times increase in electrical conductivity, a 3.7-times improvement of thermal conductivity, and a 1.7-times increase in dispersibility were achieved. We would like to note that there is still much room for improvement, as the CNTs were not oriented along the current path, but were normal to the current flow. In this regard, we envision that our approach would be suited to improve

crystallinity of SWCNT fibers since the direction of the CNT alignment and current flow could be easily matched. We believe that we have succeeded in demonstrating an approach to improve the crystallinity of SWCNTs by a post-process to overcome one of the major limitations of SWCNTs toward real application analogous to that of carbon fibers.

Experimental Methods

CNT Synthesis

SWCNT forests were synthesized in a 1" tube reactor from Al₂O₃ (40 nm) / Fe (1.8 nm) catalysts sputtered on silicon wafers with ethylene (100 sccm) and water (~100–200 ppm) using He with H₂ as carrier gases at a total flow of 1 liter per minute at 750 °C. The forest consists of aligned SWCNTs with high selectivity (99% single wall) and was very sparse (mass density: ~0.04 g/cm³).²⁹

Characterization

Raman G- to D-band ratios of the SWCNT sheets were characterized by Raman spectroscopy using a Thermo-Electron Raman Spectrometer at an excitation wavelength of 532 nm. The electrical and thermal properties were characterized as previous report.^{30,31} Electrical conductivity of the fabricated aligned SWCNT sheets was calculated from the measured sheet resistance using a commercial four probe electrical measurement tester (Mitsubishi chemical, Loresta-EP MCP-T360) and the average cross-sectional height. Thermal diffusivity (in plane) of SWCNT sheets was measured at room temperature in air by a thermowave analyzer (TA3, Bethel Co., Ltd). The specific heat was estimated by differential scanning calorimetry (DSC, EXSTAR X-DSC7000, Hitachi High-Tech Science Corporation). The change in wall number and diameter of CNTs were evaluated by transmission electron microscopy (TEM, TOPCOM

EM-002B). The number of SWCNTs used in the TEM estimation of the diameter and wall number (n) is n=87 of as-grown, n=82 of *heat*, n=80 of *heat¤t*.

Acknowledgments

This paper is based on results obtained from a project commissioned by the New Energy and Industrial Technology Development Organization (NEDO). We acknowledge support from Technology Research Association for Single Wall Carbon Nanotubes (TASC). The authors are grateful for S. Ishizawa for technical assistance.

Notes and References

1. I. Mochida, S. H. Yoon, N. Takano, F. Fortin, Y. Korai and K. Yokogawa, *Carbon*, 1996, **34**, 941–956.
2. M. Minus and S. Kumar, *JOM*, 2005, **57**, 52–58.
3. F. Tanaka,; T. Okabe, H. Okuda, M. Ise, I. A. Kinloch, T. Mori and R. J. Young, *Carbon*, 2013, **52**, 372–378.
4. S. Chand, *J. Mater. Sci.*, 2003, **35**, 1303–1313.
5. W. Ma, L. Liu, R. Yang, T. Zhang, Z. Zhang, L. Song, Y. Ren, J. Shen, Z. Niu, W. Zhou and S. Xie, *Adv. Mater.*, 2009, **21**, 603–608.
6. Y. Xia, M. Zhao, Y. Ma, M. Ying, X. Liu, P. Liu and L. Mei, *Phys. Rev. B*, 2002, **65**, 155415.
7. N. Behabtu, C. C. Young, D. E. Tsentelovich, O. Kleinerman, X. Wang, A. W. K. Ma, E. A. Bengio, R. F. Waarbeek, J. J. Jong, R. E. Hoogerwerf, S. B. Fairchild, J. B. Ferguson, B. Maruyama, J. Kono, Y. Talmon, Y. Cohen, M. J. Otto and M. Pasquali, *Science*, 2013, **339**, 182–186.
8. L. Shi, D. Li, C. Yu, W. Jang, D. Kim, Z. Yao, P. Kim and A. Majumdar, *J. Heat Transfer*, 2003, **125**, 881–888.

9. M. Grujicic, G. Cao and W. N. A. Roy, *J. Mater. Sci.*, 2005, **40**, 1943–1952.
10. X. Wang, N. Behabtu, C. C. Young, D. E. Tsentelovich, M. Pasquali and J. Kono, *Adv. Func. Mater.*, 2014, **21**, 3241–3249.
11. C. Subramaniam, T. Yamada, K. Kobashi, A. Sekiguchi, D. N. Futaba, M. Yumura and K. Hata, *Nature Communications*, 2013, **4**, 2202–2208.
12. S. J. Tans, H. Devoret, A. Thess, R. E. Smalley, L. J. Geerligs and C. Dekker, *Nature*, 1997, **386**, 474–477.
13. E. T. Thostenson, Z. Ren and T. W. Chou, *Compo. Sci. Tech.*, 2001, **61**, 1899–1912
14. E. Joselevich, H. Dai, J. Liu and A. H. Windle, *Carbon nanotubes, Topics Appl. physics III*, ed. A. Jurio, M. S. Dresselhaus and G. Dresselhaus, Springer, Verlag Berlin Heidelberg, 2008, pp 101–106.
15. A. Govindaraj and C. H. R. Rao, *Carbon Nanotechnology*, ed. L. Dai, Elsevier B. V. Amsterdam, 2006, pp 22–33.
16. A. G. Nasibulin, A. Moisala, D. P. Brown, H. Jiang and E. I. Kauppinen, *Chem. Phys. Lett.*, 2005, **402**, 227–232.
17. K. Koziol, M. Shaffer and A. H. Windle, *Adv. Mater.*, 2005, **17**, 760–763.
18. T. Saito, S. Ohshima, T. Okazaki, M. Yumura and S. Iijima, *J. Nanosci. Nanotechnol.*, 2008, **8**, 6153–6157.
19. H. Kimura, J. Goto, S. Yasuda, S. Sakurai, M. Yumura, D. N. Futaba and K. Hata, *J. Am. Chem. Soc.*, 2013, **7**, 3150–3157.
20. M. Endo, Y. A. Kim, T. Hayashi, K. Nishimura, T. Matsusita, K. Miyashita and M. S. Dresselhaus, *Carbon*, 2001, **39**, 1287–1297.
21. D. Mattia, M. P. Rossi, B. M. Kim, G. Korneva, H. H. Bau and Y. Gogotsi, *J. Phys. Chem. B*, 2006, **110**, 9850–9855.
22. J. Zhao, Y. Zhang, Y. Su, X. Huang, L. Wei, E. S. W. Kong and Y. Zhang, *Diamond Related Mater.*, 2012, **25**, 24–28.

23. R. Jin,; Z. X. Zhou, D. Mandrus, I. N. Ivanov, G. Eres, J. Y. Howe, A. A. Puzos and D. B. Geohegan, *Physica B*, 2007, **388**, 326–330.
24. S. Musso, M. Giorcelli, M. Pavese, S. Bianco, M. Rovere and A. Tagliaferro, *Diamond Related Mater.*, 2008, **17**, 542–544.
25. M. Yudasaka, H. Kataura, T. Ichihashi, L. C. Qin, S. Kar and S. Iijima, *Nano Lett.*, 2001, **1**, 487–489.
26. M. Yudasaka, T. Ichihashi, D. Kasuya, H. Kataura and S. Iijima, *Carbon*, 2003, **41**, 1273–1280.
27. M. J. Lopez, A. Rubio and J. A. Alonso, *IEEE Trans Nanotech.*, 2004, **3**, 230–236.
28. P. Kim, L. Shi, A. Majumdar and P. L. McEuen, *Phys. Rev. Lett.*, 2001, **87**, 215502–1–4.
29. K. Hata, D. N. Futaba, K. Mizuno, T. Namai, M. Yumura and S. Iijima, *Science*, 2004, **306**, 1362–1364.
30. G. Chen, D. N. Futaba, S. Sakurai, M. Yumura and K. Hata, *Carbon*, 2014, **67**, 318–325.
31. G. Chen, D. N. Futaba, H. Kimura, S. Sakurai, M. Yumura and K. Hata, *ACS Nano*, 2013, **7**, 10218–10224.
32. M. Ouyang, J. L. Huang and C. M. Lieber, *Phys. Rev. Lett.*, 2002, **88**, 066804–1–4.
33. E. D. Minot, Y. Yaish, V. Sazonova and P. L. McEuen, *Nature*, 2004, **428**, 536–539.
34. J. H. Warner, F. Schäffel, G. Zhong, M. H. Rummeli, B. Büchner, J. Robertson and A. D. Briggs, *ACS Nano*, 2009, **3**, 1557–1563.
35. F. Börrnert, S. Gorantla, A. Bachmatiuk, J. H. Warner, I. Ibrahim, J. Thomas, T. Gemming, J. Eckert, G. Cuniberti and B. Büchner, *Phys. Rev. B*, 2010, **81**, 201401–1–4.
36. C. Jin, K. Suenaga and S. Iijima, *Nano Lett.*, 2008, **8**, 1127–1130.
37. H. Yoon, M. Yamashita, S. Ata, D. N. Futaba, T. Yamada and K. Hata, *Scientific Reports*, 2014, **4**, 3907–1–8.